ACS APPLIED MATERIALS & INTERFACES

Research Article

Cite This: ACS Appl. Mater. Interfaces 2019, 11, 15079−15087

www.acsami.org

Carbon-Based, Ultraelastic, Hierarchically Coated Fiber Strain Sensors with Crack-Controllable Beads

Siyeon Jang,[†] Jisun Kim,[‡] Da Wan Kim,[‡] Ji Won Kim,[‡] Sungwoo Chun,[†] Heon Joon Lee,[‡] Gi-Ra Yi,[*,‡] and Changhyun Pang[*,†,‡]

[†]SKKU Advanced Institute of Nanotechnology and [‡]School of Chemical Engineering, Sungkyunkwan University (SKKU), Seobu-ro, Jangan-gu, Suwon 16419, Republic of Korea

Supporting Information

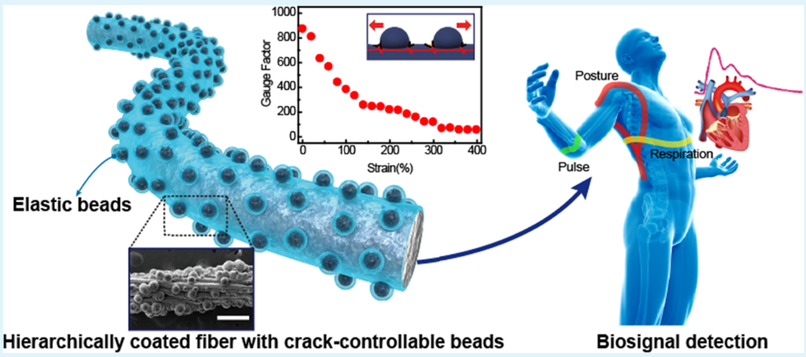

ABSTRACT: Fiber-based electronics or textronics are spotlighted as a promising strategy to develop stretchable and wearable devices for conformable machine−human interface and ubiquitous healthcare systems. We have prepared a highly sensitive fiber-type strain sensor (maximum gauge factor (GF) = 863) with a broad range of strain (ε < 400%) by introducing a single active layer onto the fiber. In contrast to other metal-based fiber-type electronics, our hierarchical fiber sensors are based on coating carbon-based nanomaterials with responsive microbeads onto elastic fibers. Utilizing the formation of uniform cracks around the microbeads, the device performance was maximized by adjusting the number of microbeads in the carbon-coating layer. We overcoated the carbon-based coating layer of the elastic fiber with a protective polymeric layer and verified no effects on the GF and the range of strain. Our fiber sensors were repeatedly tested more than 5000 times, exhibiting excellent cyclic responses to on/off switching behaviors. For practical applications, the hierarchical fiber sensors were sewed into electrical fabric bands, which are integrable to a wireless transmitter to monitor waveforms of pulsations, respirations, and various postures of level of bending a spinal cord.

KEYWORDS: *conductive fiber, hierarchical structure, biosensor, nanoparticle, crack*

INTRODUCTION

Stretchable and wearable electronics with sensory and integrable elements have brought forth revolutionary advances in ubiquitous healthcare (U-healthcare) systems and robotic platforms. Such devices can be used to monitor human motions and various biosignals, and/or incorporated into electronic skin for soft robotic systems.[1−7] Fiber-based electronics, in particular, have become attractive to be woven into textiles of wearable electronics with high adaptability and wearability for the human body. Fiber-based electronics have been used to produce reversibly stretchable conductors,[8,9] actuators,[10,11] and strain sensors.[12−14] Conductive fibers with high sensitivity and flexibility have been applied to sensor devices to monitor changes in electric signals (e.g. resistance or capacitance) on various platforms.[15−17] Among such devices, fiber-type piezoresistive sensors demonstrated low energy consumption, simple device structures, and easy read-out mechanisms.

Fiber-type sensors capable of piezoresistive strain can translate mechanical elongation into electric signals, which can be useful for time-dependent monitoring of very small structural deformations in the stretchable fibers. To fabricate such fiber-based devices, various materials have been utilized in their active layers, including metal nanostructures,[14,18,19] conductive polymeric materials,[20−22] and carbon-based materials.[13,23,24] In most initial reports, inorganic conductive materials (e.g., particles or wires of Ag, Au, Ni, or ZnO) were implemented in resistive fiber-type wearable sensors for vitro/in vivo medical devices (e.g., smart gloves) and soft-robotics.[14,18,19,25] Such metal- or oxide-based fiber-type sensors demonstrated high sensitivity [gauge factor (GF) > 100], responsiveness to reversible strain, and excellent electrical/mechanical properties

Received: February 20, 2019
Accepted: March 28, 2019
Published: March 28, 2019

DOI: 10.1021/acsami.9b03204
ACS Appl. Mater. Interfaces 2019, 11, 15079−15087

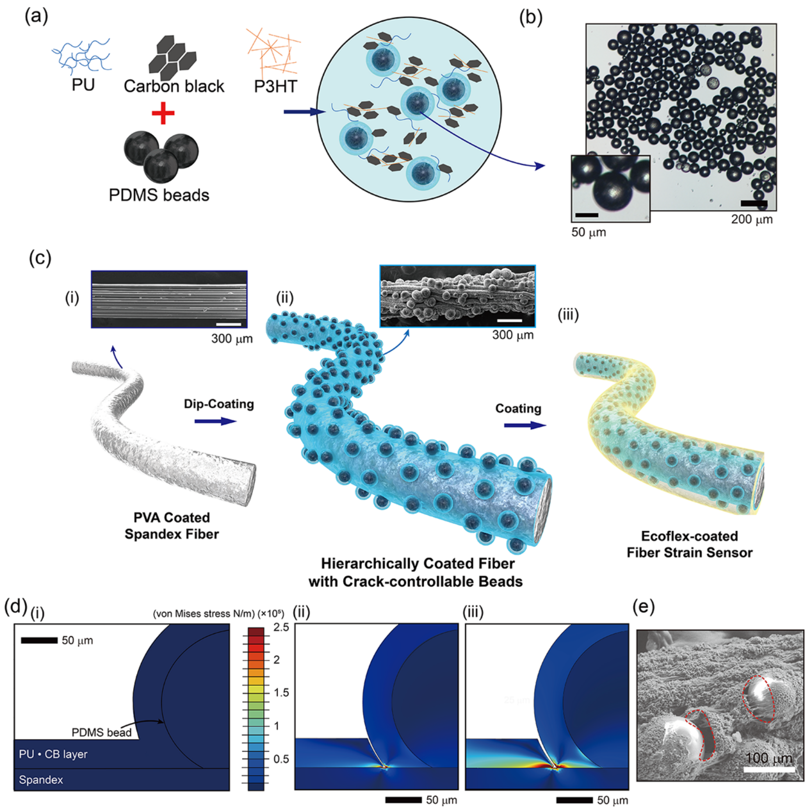

Figure 1. (a) Schematic illustration of preparing the conductive paste. (b) Optical microscopy image of the PDMS beads. (c) Schematic illustration of fabricating the fiber strain sensor. Inset images show SEM images of the fiber before (i) and after (ii) coating with the conductive paste. (d) FEM simulation of the strain regulation effect on a microbead of the coated fiber. (e) SEM image of the fiber surface employed with beads and cracks when strain is applied. Red dotted lines indicate the deformation of the microcracks after the applied strain.

(stretchable strain > 100%), owing to numerous reversible contacts generated effortlessly between the inorganic materials and polymeric fiber interfaces.[19] Despite striking performances of these metal- or oxide-based devices, rare earth metals (Ag, Pt, or Au) are expensive and require sophisticated or costly methods such as electro-plating spinning,[21] thermal and chemical vapor deposition,[26] electrochemical deposition,[10] and chemical reduction with acidic wastes.[19,24] Alternatively, carbon-based materials have also been utilized as active sensory layers, which include carbon nanotubes, carbon black (CB), and graphene oxides. Coating carbon-based solutions with binders onto the polymeric fiber to fabricate resistive strain sensors is simple, reliable, and cost-effective. However, such carbon-based fiber-type devices have relatively low sensitivity and narrow sensing ranges because of low adhesion between the carbon-based materials and polymeric layers.[27] To overcome this issue, carbon nanotube-based hierarchical architectures were introduced through multistep processing (e.g., coating and twisting) on a polymeric fiber to present exceptionally versatile and super-plastic electronics.[28]

In terms of structural features, fiber-type sensors with smooth surfaces have homogenous strain distribution during deformation, limiting the sensing range and sensitivity of the device.[26] Hence, much effort has been devoted to producing various designs of the fiber surface to control the strain applied and significantly improve sensor performances.[24,26−28] A graphene-based fiber with spring-like architectures exhibited a wide sensing range, fast signal response, and high sensitivity, but its stretchability is insufficient to monitor human motions induced by multiple joints with strains usually larger than 100%.[24] Moreover, the propagation of multiscale cracks on the structured fiber surfaces via stretching has recently demonstrated a significant increase in electrical resistance by forming gaps between the crack edges.[26,37] On the basis of such a principle, a bead-structured polymeric fiber coated with a thin gold layer showed surface strain redistribution through its structural designs and formation of cracks to enhance its sensitivity even under large mechanical deformations.[26] Such beads on the fiber surface, however, need to be intrinsically aligned to attain meticulous structural uniformity for the desired strain redistribution and sensitivity.

In this article, we demonstrated a highly sensitive fiber-type strain sensor fabricated through a facile dip-coating method of a polyurethane (PU)-based coating solution consisting of CB nanoparticles, poly(3-hexylthiophene-2,5-diyl) (P3HT), and elastic polydimethylsiloxane (PDMS) microbeads (~100 μm in diameter). CB nanoparticles are hierarchically scattered on the microbeads, which are dispersed on the fiber surface by the as-mentioned coating method, whereas cracks are uniformly distributed around the bead architectures upon applied preload. After coating a protective layer, our hierarchically coated fiber-type sensor showed remarkably high sensitivity (the maximum GF = 863), a wide strain range up to 400%, and reversibility. The performances of the device can be controlled by changing the content of the microbeads in the coating agent. Furthermore, we could obtain highly repeatable and reproducible signals over multiple cyclic tests (>5000 cycles) with fast response time under well-defined on/off stretching behaviors (<400%). For medical applications, our fiber-type sensor can monitor waveforms of pulsations retrieved from an artificial arm with

DOI: 10.1021/acsami.9b03204
ACS Appl. Mater. Interfaces 2019, 11, 15079−15087

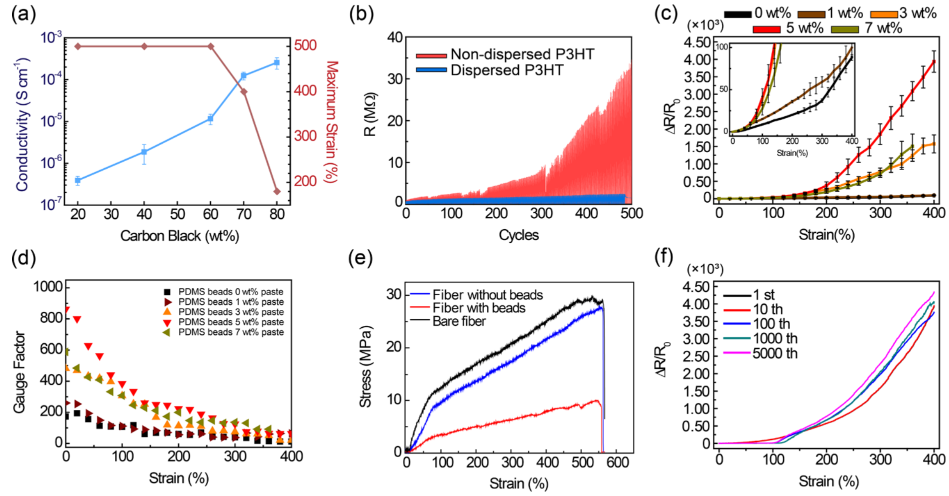

Figure 2. (a) Dependence of the initial conductivity and maximum strain before electrical failure of the hierarchical fiber with varying CB nanoparticle contents. (b) Measurements in electrical resistance with repeated strains of 400% over 500 cycles for the fiber with/without P3HT. (c) Relative changes in electrical resistance up to 400% strain for the fiber with varying PDMS microbead contents within the conductive paste. The inset graph focuses on the relative changes in electrical resistance for fibers coated with paste containing 0 and 1 wt % of microbeads. (d) GF of the fibers coated with pastes of varying PDMS bead contents up to 400% strain. (e) Stress−strain curves for a bare fiber and a coated fiber with/without microbeads. (f) Durability testing of the fiber sensor coated with conductive paste of 5 wt % microbeads.

varied blood pressures (low, normal, and high levels). After knitting our fiber sensor into a textile, various postures in response to distortions of a human spinal cord (e.g., bent or straightened state) and the number of respirations of volunteers can be monitored, shedding light on potential uses in orthotherapy or surgical correction.

RESULTS AND DISCUSSION

Fabrication of Hierarchical Fiber Sensors with PDMS Beads. Figure 1a−c shows schematic illustrations of fabricating the hierarchical fiber strain sensors by coating a conductive paste composed of the PU elastomer, CB nanoparticles, P3HT, and PDMS microbeads. The PDMS beads were synthesized by Shirasu porous glass membrane emulsification (see Figures 1b, S3, and the Methods section for fabrication details). CB nanoparticles are the conductive filler in the PU/CB matrix, whereas P3HT molecules increase the molecular interactions among the CB nanoparticles for enhanced electrical properties.[29,38] As shown in Figure 1c, the conductive suspension was coated on a surface-treated, stretchable polymeric fiber through a facile dipping method (see Figures S4 and S5 for conductive pastes). The PDMS microbeads (ave. ≈ 100 μm in diameter) dispersed on the fiber surface are hierarchically scattered with CB nanoparticles to derive the conductive hierarchical fiber (see the inset images of Figure 1c and the Methods section for fabrication details). The distribution of the bead architectures can be modified by changing the ratio of PDMS beads in the coating agent. In our observation, cracks can be generated around the edge of the bead architectures because of localized stress under applied strain [see Figure 1d(i−iii) and the scanning electron microscopy (SEM) image of Figure 1e]. With numerous cracks on the conductive fiber, an elastic protective layer of Ecoflex was laminated on top of the fiber surface (∼100 μm in thickness), as shown in Figure 1c. We assumed that the sensitivity of the fiber sensor can be controlled by altering the crack distribution around the bead architectures. This is because, according to the mechanism of crack propagation, the electrical conduction of the strain sensor may be drastically restricted by the separation of crack edges upon stretching.[37] This behavior will be discussed later. Moreover, the cracks on the conductive fiber may disperse the stress induced by the applied strain for higher stretchability without serious delamination.

Electrical and Mechanical Characteristics of the Hierarchical Fiber Sensors. First, we investigated the changes in the conductivity for the fibers coated with varied CB nanoparticle contents in the conductive paste (20−80 wt %). As shown in Figure 2a (blue line), the conductivities of the fiber significantly improved with increasing the content of the conductive filler (CB nanoparticles) in the coating paste. Meanwhile, the maximum stretchability of the conductive fibers (strain until irreversible rupturing) decreased when increasing the content of CB nanoparticles (see red line of Figure 2a). On the basis of our experiments, we used conductive fiber with 70 wt % of the CB filler (maximum reversible stretchability ∼400%) for appropriate operating and sensing range (10^{-4} to 10^{-5} S cm^{-1}) of piezo-resistive sensors.[24,30] We added P3HT into the PU/CB paste (CB/P3HT = 1:0.05) to improve the repeatability of the fiber (∼400% of elongation) and prevent delamination of the coating layer as shown in Figures 2b and S6. These results are mainly attributed to P3HT acting as a binder among conductive materials in the PU/CB matrix, which increase the $\pi-\pi$ interactions for the uniform dispersion of the CB nanoparticle clusters.[31,38]

We then varied the PDMS bead content (0−10 wt %) in the conductive pastes to understand their distribution effect on the surface of the fiber. We utilized scanning electron microscopy (SEM) imaging (see the SEM images of Figures S7 and S9) and the measurements of the distance in-between the coated beads verify the uniform dispersion throughout the fiber (Figure S8). The number of beads coated on the fiber sensor was counted according to the mass percentage of the beads. We confirmed that the quantity of beads actually coated increased with the quantity of beads added to the coating solution. The distance between the particles of each grain in the 5 wt % sample was relatively uniform (∼10 μm) across the surface. Therefore, the number and uniformity of beads on the hierarchically coated fibers were highly dependent on the content of microbeads in

DOI: 10.1021/acsami.9b03204
ACS Appl. Mater. Interfaces 2019, 11, 15079−15087

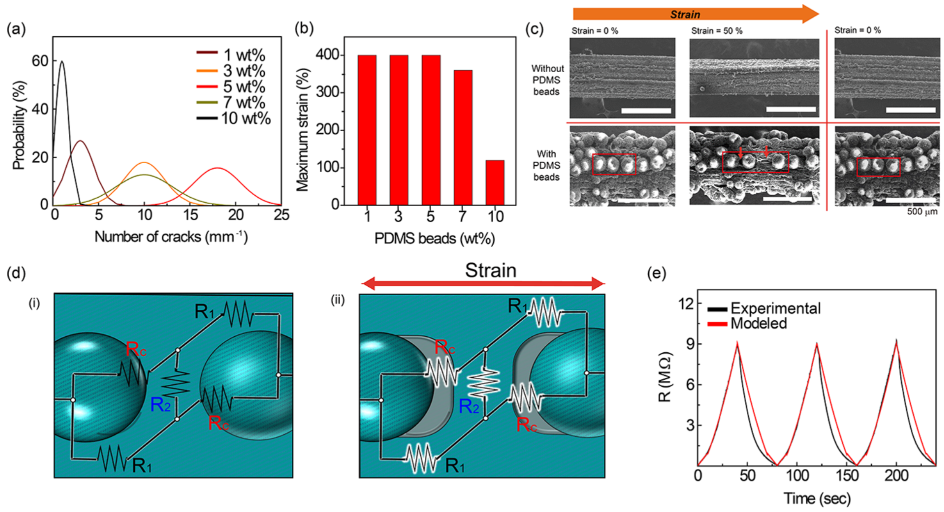

Figure 3. (a) Distribution of crack formation probability according to the number of cracks with different PDMS bead contents within the coating agents. (b) Maximum strain (%) applied before electrical failure for the hierarchical fiber sensor with variable PDMS bead weight ratios in the conductive pastes. (c) SEM images which investigate the strain regulation effect of the beads on the hierarchically coated fiber sensor as compared to that on a coated fiber sensor without microbeads. (d) Schematic illustrations of the basic circuit within the fiber strain sensor with beads (i) before and (ii) after strain is applied. (e) Comparison of modeled and experimental results of electrical resistance for the strain sensor-coated paste containing 5 wt % of PDMS beads through 400% strain applied.

the coating agents. To create cracks around the beads, an initial strain (<400%) was applied to the fiber with beads and coated with Ecoflex. As shown in Figure 2c, the relative change in resistance ($\Delta R/R_{\mathrm{off}}$) was plotted as a function of the applied strain (0−400%) and consequently the fiber coated with paste containing 5 wt % of PDMS beads showed the most dramatic changes in resistance within the strain-applied range of 400%. Because the evaluation of sensitivity from the previous GF, which depended on the initial resistance values of strain sensors, was questionable, we justified the sensitivity of the fibers through the re-estimated GF, defined as GF = $(1/R_n)(R_{n+1} - R_n/\varepsilon_{n+1} - \varepsilon_n)$ (see the Supporting Information for details).[39] The fiber coated with paste containing 5 wt % of PDMS beads showed dramatic improvements in sensitivity (the maximum GF = 863) up to strain of 400%, owing to the generation of cracks within the microbeads (see Figure 2d). Furthermore, the fiber coated with paste containing 5 wt % of PDMS beads was highly sensitive also in relatively low strains to be applicable to monitor human motion and various biological signals. Owing to the increase of the sensor's resistance when the applied strain increases, the GF of the fiber strain sensors displays a tendency to decline. On the other hand, the fiber coated with paste containing 7 wt % of microbeads exhibited lowered sensitivity, attributed to their excessive amount (results for this will be discussed later in detail). In addition, the mechanical properties of the PU/CB-coated fibers with or without microbeads (5 wt %) and a bare fiber are depicted in Figure 2e. The coated fiber with beads shows a relatively lower stress than the fiber coated with paste without beads. This is related to the effect of strain dispersion owing to the generation of cracks among the beads. Applying a protective layer of Ecoflex onto the fiber coated with the optimized conductive paste (5 wt % of microbeads), our fiber sensor showed stable responses to electrical signals up to 5000 cycles without a notable degradation (see Figure 2f).

To study the effect of cracks formed around the beads of the fiber, we investigated the crack probability and electromechanical properties by changing the weight ratio of the microbeads in the coating agents (see Figure 3a,b). After coating the conductive paste with 5 wt % of microbeads on the stretchable fiber and applying prestrain (~400%), the number of cracks generated (ave. ≈ 18 #mm^{-1}) was maximized as plotted in Figure 3a. This is because the number of beads directly in contact with the fiber increases up to the coating agent with 5 wt % of microbeads. In the case of the paste with 10 wt % of microbeads, however, the amount of microbeads coated onto the fiber is superfluous, which causes multilayering of the beads and easily breaks their electrical connections (see Figure S9). On the basis of such behaviors, the maximum strain of the device without electrical failure decreased drastically for fibers coated with paste containing 10 wt % of microbeads, as shown in Figure 3b. Moreover, we investigated that the crack size shows negligible changes to an applied strain of 50%, indicating trivial dependency with the bead's mass fraction in the paste (see Figure S10).

After obtaining a uniform dispersion of cracks on the hierarchically coated fiber sensor with beads (paste with 5 wt % of microbeads), we set a simple model to understand the reversible and linear changes of its electrical signals. We examined the structural changes on the conductive hierarchical fiber before and after the strain (~50%) (see Figure 3c). The cracks were created around the bead architectures of the fiber, whereas microscale cracks were not examined on the coated fiber without beads. Upon stretching the fiber sensor, reversibly fractured gaps (see red arrows) around the beads were observed, wherein such gaps and resistivity responded linearly to the applied strain (see Figure 3d,e). As illustrated in Figure 3d, such behaviors can be explained with a simplified model[6] to describe the resistance of the fractured surface

$$R = \frac{R_1R_2 + 2R_1R_c + R_2R_c}{R_1 + 2R_2 + R_c} \quad (1)$$

Here, R_1, R_2, and R_c are the resistances of the CB/PU composite, the bridge between cracks, and a single crack, respectively. Because R_c suppresses R_1 and R_2 under the applied strain, total R can be expressed as $R \approx 2R_1 + R_2$. Fitting in experimental results into the equation, total R can be 9.26 (kΩ/%) × strain (%) +

DOI: 10.1021/acsami.9b03204
ACS Appl. Mater. Interfaces 2019, 11, 15079−15087

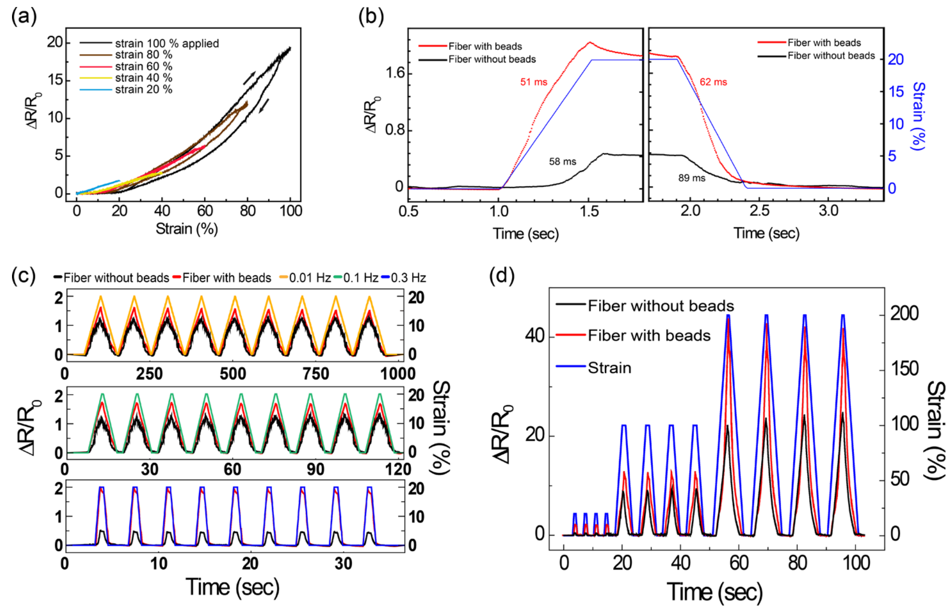

Figure 4. (a) Hysteresis of the hierarchical fiber sensor according to the varying strains applied. (b) Comparison of resistive responses of the coated fiber sensor with/without PDMS beads to loading (20%) and unloading (0%) of the mechanical strain. (c) Resistive response of the fiber sensor against the repeated strain of 20% with different hertz of 0.01 Hz (yellow), 0.1 Hz (green), and 0.3 Hz (blue). (d) Time-dependent resistive responses of the strain sensor to repeated strains of 20, 100, and 200%. Here, all fiber strain sensors with hierarchical bead architectures were coated with the optimized conductive paste (5 wt % of PDMS beads in the coating agent).

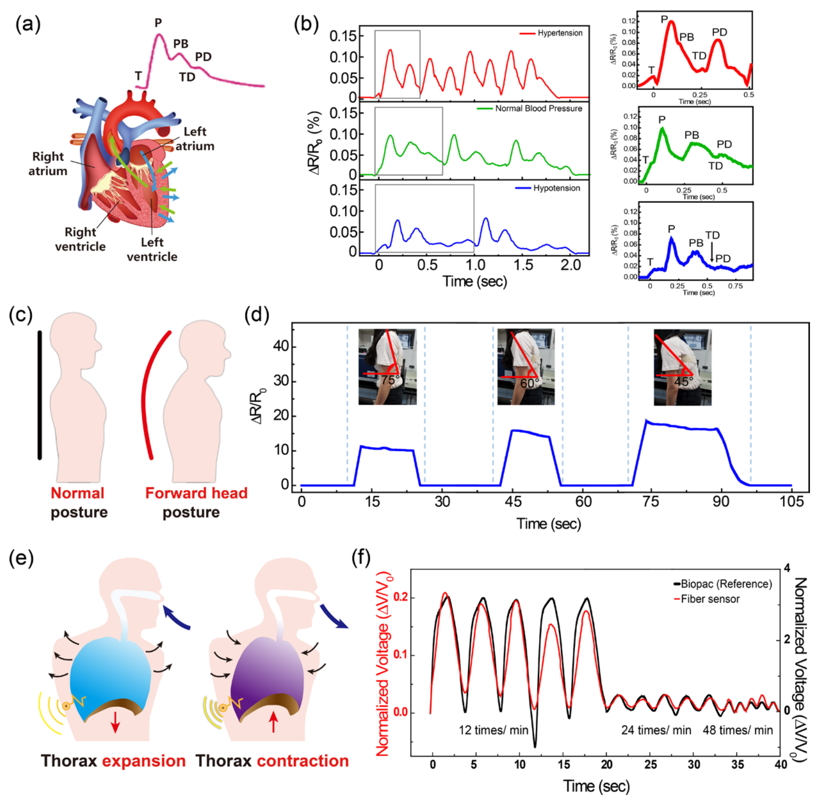

Figure 5. (a) Schematic illustration of measuring waveforms corresponding to pulse signals from an artificial cardiac system. (b) Resistive responses to pulse signals in conditions of hypertension, normal blood pressure, and hypotension. The left graph was filtered by fast Fourier transform with a band pass filter for pulse shapes of different cardiovascular pulses (1.0 Hz < band pass filter < 8.0 Hz). (c) Schematic illustration of the posture in the reference and comparison conditions with the difference angle. (d) Resistive responses of the fiber strain sensors in the posture corrector for various bending angles of a human spine. (e) Schematic illustration of a human respiration mechanism. (f) Time-dependent relative changes in voltage for human respiration.

30.6 kΩ under 100% strain (R_1 = 15.3 kΩ and R_2 = 9.26 (kΩ/%) × strain (%)), and 29.0 (kΩ/%) × strain (%) − 2870 kΩ at more than 100% strain (R_1 = 15.3 kΩ and R_2 = 29.0 (kΩ/%) × (strain − 100) (%)) (see the Supporting Information for details). The

DOI: 10.1021/acsami.9b03204
ACS Appl. Mater. Interfaces 2019, 11, 15079−15087

conductive layer of the bridge between cracks lengthens substantially over 100% strain. Consequently, the value of R_2, which follows a linear function, is influenced by the change in the percolation network, showing an increase in resistance greater rather than that up to 100% of strain applied. This gives rise to the linear behavior of our presented strain sensor. Hence, complying with the as-mentioned model, our fiber strain sensor with microbeads exhibits linearity in two separate phases up to 400% strain. With this assumption, our model is well in agreement with the experimental results (see Figure 3e).

Furthermore, hysteresis of the fiber sensor was measured for various strains (20−100 and 400%) as shown in Figure 4a (see Figures S11 and S12). The hierarchical structure with beads makes cracks form on the strain sensor; as a result, these cracks act on improving the hysteresis performance. The viscoelastic property between the fractured surfaces of the cracks is attenuated, improving response performances of the cracked fiber sensor. In accordance with its high performance with dynamic strains, the response time of the hierarchical fiber sensor with beads (62 ms) was faster than the device without beads (89 ms) (see Figure 4b). These results can be attributed to the cracks induced by the hierarchical structure with microbeads because of the easy disconnection−reconnection of the fracture surfaces with minimal viscoelastic behavior.[40] With regards to frequency responses (Figure 4c), output signals of the bead-loaded device were rapidly detected and distinguishable with minimal delay times for various frequencies (0.01, 0.1, and 0.3 Hz). A time-resolved scan of the applied strain (<200%) and output signals were additionally investigated as shown in Figure 4d, indicating improved sensitivity and responsiveness of the hierarchical fiber sensor with beads. Meanwhile, the minute, sharp peaks (red line in Figure 4c,d) are attributed to the negligible hysteresis in between the signals of the relative change in resistance. This is owed to the viscoelastic deformation of both fiber and the coated layer of the PU/CB matrix.

Potential Applications into Wearable Textronics for Healthcare Monitoring. To demonstrate the potential of our fiber sensors in wearable devices, we produced various textiles by weaving the fiber to detect a tiny portion from its wide sensing range, and monitor waveforms of the brachial artery pulses as shown in Figure 5a. Pulse data were measured from the identical contact spot of a blood pressure assessment apparatus (BT-CEAB II, BT Inc.), denoted with an arrow in the inset images of Figure S13 (see the Supporting Information for detailed measurement). On the basis of clinical data from patients, the apparatus is known to regulate various pulse waveforms of hypertension, normal blood pressure, and hypotension by manipulating its controller.[32] The electric band (E-armband) sewed with our fiber sensor has high flexibility and stretchability. This enables the E-armband to conformally contact the apparatus without using a sticky medical tape. As shown in Figure 5b, pulse signals were detected for three different conditions (hypertension, normal blood pressure, and hypotension) against time, from which distinct frequencies and waveforms corresponding to various peaks and cardiac motion could be differentiated (see the inset illustrations of Figure 5a). In Figure 5b, graphs on the right depict physiological features detected from points of a human wrist pulse waveforms (e.g. *T* point, *P* point, *PB* point, *TD* point, and *PD* point),[41] which provide meaningful biomedical information for healthcare diagnosis. Furthermore, the real-time human pulsation could be measured through contact with the E-armband and a pulse spot on the human wrist as shown in Figure S14.

We also developed an electronic band-type posture corrector (E-posture-corrector) with our fiber sensor to continuously measure resistive changes to bending angles of a human spinal cord. The fiber sensor vertically sewed onto a fibrous band showed excellent compliance with the embedded textiles, as shown in Figure S15a(i). We then confirmed excellent integrability of our device with a wireless transmitter, as well as wearability for our newly designed E-posture-corrector with minimal signal distortions during diagnosis [see Figure S15a-(ii)]. With the E-posture-corrector equipped onto the volunteer's back, we measured signals against time with varying bending angles (θ) of the volunteer's spine as displayed in Figure 5c,d (see the Methods section and Figure S15b,c for a detailed analysis of θ, strain, and electric signals). Collection of clinical information from the E-posture-corrector may be useful for orthotherapy to improve one's posture, prevent slouching, and align his or her spine to relieve pain and discomfort. Such a procedure may potentially be applied to the surgical management of patients with acute spinal cord injury, and/or medical devices to monitor the distortion levels of the spinal cord during surgery.[33] In addition, our fiber sensor can be horizontally sewed onto an E-band to monitor waveforms of respirations from a volunteer in various breathing conditions (fast, normal and, slow breathing rate) (see Figure S16). As shown in Figure 5e,f, our experimental data (yellow line) are well in agreement with results (black line) measured using a commercial breathing sensor (Biopac.) (see the Methods section). With further optimization, we envision that our fiber sensor system could be integrated with wearable biosignal-monitoring devices to evaluate the breathing quantities (e.g., respiration volume and lung capacities).

■ CONCLUSIONS

We propose a highly sensitive (the maximum GF = 863) fiber-type strain sensor with a broad sensing range (ε < 400%) and excellent durability (<5000 cycles), fabricated by dip-coating carbon-based nanomaterials and PDMS microbeads onto the stretchable fiber. Our approach to coating the conductive paste and employing bead architectures is facile, cost effective, and does not involve any metallic nanomaterials (Ag or Au nanowire/nanoparticle). To maximize the performances of the device, we adjusted the number of microbeads in the coating agent for uniform distribution of cracks on the fiber, and retrieved experimental results well in agreement with our predictions. For practical applications, the hierarchical fiber sensors with beads were weaved into different types of textronics to detect waveforms of pulsations and various postures through a wireless transmitter (level of bending a spinal cord and waves of respirations). On the basis of these demonstrations, our design of a fiber-type strain sensor may develop innovative strategies for potential applications in advanced wearable electronics and textronics with diagnostic and/or therapeutic functionalities.

■ METHODS

Preparation of the Conductive Paste. PU (0.27 g, Sigma-Aldrich) was dispersed in 20 g of chloroform (Daejung Chemicals, Siheung-si, Gyeonggi-do, South Korea) via mild sonication in deionized (DI) water at 60 °C for 30 min. The dispersant, 0.077 g of P3HT (Sigma-Aldrich) was then dissolved in the solution followed by bath sonication for 10 min. After P3HT was completely dispersed throughout the solution, the color of the solution turned orange. Then, 0.63 g of CB nanoparticles (CB, Raven 1170, Columbian) (PU/CB = 3:7 in weight ratio), the conductive filler, was dispersed in the solution via vortex mixing and bath sonication for 30 min. From then, 0.21, 0.64, 1.1, 1.5, 2.3 g of PDMS beads (resembles 1, 3, 5, 7, 10 weight percent (wt %) of the whole solute, respectively) were added into the mixture solution. The solution was mixed vigorously using the vortex mixer followed by bath sonication for 10 min (see Figures 1a, S4, and S5).

In the case of conductive pastes without PDMS beads, solutions with weight ratios of PU/CB = 2:8, 3:7, 4:6, 6:4, 8:2 were prepared by mixing 0.18 g:0.72 g (0.18 g of PU and 0.72 g of CB), 0.27 g:0.63 g, 0.36 g:0.54 g, 0.54 g:0.36 g, and 0.72 g:0.18 g in 20 g of chloroform, respectively (see Figure 2a).

Fabrication of Fiber Strain Sensors. To fabricate highly stretchable fiber strain sensors, PU-based stretchable spandex fibers (diameter 300 μm; Kwangrim Textile, Dalseo-gu, Daegu-kwangyeoksi, South Korea) with 500% stretchability in the horizontal direction were used as stretchable substrates of the fiber sensors. The fibers underwent additional processes to enable stable attachment of the conductive paste onto the surface of the stretchable fiber even under applied strain. The fibers were first treated with the oxygen plasma for 2 min to make the fiber surfaces hydrophilic by forming hydroxyl functional groups (−OH) on the fibers.[34] Then, the plasma-treated fibers were immersed into a PVA (polyvinyl alcohol, Sigma-Aldrich) 5 wt % solution in DI water for 30 s. To prepare the PVA 5 wt % solution, 2.11 g of PVA was dissolved into 40 g of DI water by stirring with a magnetic bar at 90 °C for 2 h. After the solvent of the PVA solution was evaporated from the fibers for 5 min, the fibers were treated again with oxygen plasma for 2 min and dipped in conductive pastes (containing 0, 1, 3, 5, 7, 10 wt % of PDMS beads, PU/CB = 3:7 in weight ratio) for 20 min via mild sonication to prevent the aggregation of CB and PDMS beads for nonuniformity (see Figures S7 and S9). To remove from the coating paste, the tips of the coated fibers were hung on an electric motor and pulled out from the coating paste at a constant speed (2 mm/s) for maximized uniformity. Through PVA and oxygen plasma treatment on the fibers, the bonds between the fibers and the conductive layer strengthened. Hydrogen bonds from the PVA treatment allowed high stability of the conductive layer even under applied strain.[35] Consequently, the conductive layer of the PVA and oxygen plasma-treated fiber returned to its original state after applying the strain, whereas the conductive layer coated directly on the fiber delaminated with the strain.

After dipping the fibers into the conductive pastes, they were dried at 70 °C for 20 min. Lastly, we covered Ecoflex (Ecoflex 00-30; Smooth-On, Inc.) on the surfaces of the fibers to protect the conductive layer. Ecoflex containing parts A and B were mixed in a 1:1 mass ratio inside a mixing container. After sufficient stirring of the mixture, the fibers coated with conductive pastes were immersed in the Ecoflex solution and cured at 80 °C for 2 h.[36] (see Figure 2c) The diameter in the final samples was around 500 μm.

Simulation Using the Finite Element Method. The finite element method (FEM) simulation analysis was performed through a commercial software (COMSOL Multiphysics version 5.2a, license number 5084832, Altsoft, South Korea) to investigate the deformation behavior of the hierarchical fiber with microbeads during tensile stretching. We used a two-dimensional model to simplify the model for a fiber coated with a PDMS microbead of 100 μm size and a conductive layer comprising PU with a thickness of 20 μm, CB, and P3HT (Sigma-Aldrich). The model was automatically meshed with a free triangular element of meshes in sizes ranging from 0.0007 to 3.5 μm. We assumed all materials to have linearly elastic properties. One edge of the fiber with PDMS beads was fixed, whereas the other edge stretched along the x-axis direction. Symmetric boundary conditions were applied to the y-axis with the fixed edge of the fiber see Figure 1d).

Characterization of Performance and Structure of the Fiber Strain Sensor. The electrical resistance of the fiber strain sensor was measured at a constant current of 0.1 mA using a Source Meter after (PXIE-1073) eliminating the contact resistances between the fibers and the device. The loading of tensile strain was performed with a custom-built equipment (Neo Plus, South Korea). Surface morphologies were examined using a field-emission scanning electron microscope (Hitachi, S-4300).

Pulse Measurements. To confirm various types of pulse, we used a Blood Pressure Assessment Trainer II (BT-CEAB II, BT Inc.) to regulate conditions of hypertension, normal blood pressure, and hypotension by adjusting the pulse rate and blood pressure through the controller of the apparatus. The fiber strain sensor was attached to the cuff of the blood pressure assessment apparatus as shown in Figure S13. We set the hypertension condition (pressure of systole: 200 mmHg, pressure of diastole: 135 mmHg, pulse rate: 100 bpm), normal condition (pressure of systole: 135 mmHg, pressure of diastole: 90 mmHg, pulse rate: 90 bpm), and hypotension condition (pressure of systole: 80 mmHg, pressure of diastole: 55 mmHg, pulse rate: 75 bpm) to conduct such experiments. Moreover, for real-time detection of human pulsation, the fiber sensor was sewed with the electric band to measure the pulse by contact with the pulse spot of a human wrist (Figure S14).

■ ASSOCIATED CONTENT

Ⓢ Supporting Information

The Supporting Information is available free of charge on the ACS Publications website at DOI: 10.1021/acsami.9b03204.

> Simplified model and mechanism of the fiber strain sensor with microbeads; preparation of the PDMS microbeads using membrane emulsification and photographs of the PDMS microbeads; preparation and photographs of the conductive pastes; fabrication of the hierarchical fiber strain sensors; finite element analysis for the deformation behavior of the hierarchical fiber with beads during tensile stretching; surface analysis of the conductive hierarchical fibers coated with the pastes containing different mass fractions of PDMS beads through SEM; uniformity analysis by obtaining the number of beads per unit length and distribution according to distance between beads with different mass fractions of PDMS beads; hysteresis performances of the fiber strain sensors; pulse test, posture sensor test, and respiration test for the fiber strain sensor (PDF)
>
> Respiration measurements using the fiber strain sensor and the reference sensor (AVI)

■ AUTHOR INFORMATION

Corresponding Authors

*E-mail: yigira@skku.edu (G.R.Y.).
*E-mail: chpang@skku.edu (C.P.).

ORCID

Gi-Ra Yi: 0000-0003-1353-8988
Changhyun Pang: 0000-0001-8339-7880

Author Contributions

S.Y., and J.K. contributed equally. S.Y., J.K., G.R.Y, and C.P. conceived the project. S.Y., J.K., and D.W.K. performed the experiments. S.Y., J.K., D.W.K., S.C., G.R.Y, and C.P. developed the experimental setup for the sensor experiments. S.Y. and J.K. performed the computational simulation for the cracking process around the microbeads on the hierarchical fiber sensor under strains. S.Y., J.K., D.W.K., S.C., and C.P designed the healthcare monitoring experiments. S.Y. and J.K. carried out these experiments. S.Y., J.K., D.W.K., G.R.Y, and C.P analyzed the data. H.J.L., S.Y., J.K., G.R.Y, and C.P. wrote the paper, and all the authors provided feedback.

Notes

The authors declare no competing financial interest.

ACKNOWLEDGMENTS

This research was supported by the Ministry of Trade, Industry & Energy (MOTIE, Korea) under the Industrial Technology Innovation Program. No. 10062694, "Development of nanomaterials hybrid fibers and bio-signal sensors for safety underwears of heavy workers". This study has been conducted with the support of the Korea Institute of Industrial Technology as "Development of smart textronic products based on electronic fibers and textiles (kitech JA-19-0001)" and the Gyeongi-Do Technology Development Program as "Development of smart textronic products based on electronic fibers and textiles (kitech IZ-19-0003)".

REFERENCES

(1) Khang, D.-Y.; Jiang, H.; Huang, Y.; Rogers, J. A. A Stretchable Form of Single-crystal Silicon for High-performance Electronics on Rubber Substrates. *Science* **2006**, *311*, 208−212.

(2) Kim, D.-H.; Lu, N.; Ma, R.; Kim, Y.-S.; Kim, R.-H.; Wang, S.; Wu, J.; Won, S. M.; Tao, H.; Islam, A.; Yu, K. J.; Kim, T.-i.; Chowdhury, R.; Ying, M.; Xu, L.; Li, M.; Chung, H.-J.; Keum, H.; McCormick, M.; Liu, P.; Zhang, Y.-W.; Omenetto, F. G.; Huang, Y.; Coleman, T.; Rogers, J. A. Epidermal Electronics. *Science* **2011**, *333*, 838−843.

(3) Matsuhisa, N.; Kaltenbrunner, M.; Yokota, T.; Jinno, H.; Kuribara, K.; Sekitani, T.; Someya, T. Printable Elastic Conductors with a High Conductivity for Electronic Textile Applications. *Nat. Commun.* **2015**, *6*, 7461.

(4) Sekitani, T.; Noguchi, Y.; Hata, K.; Fukushima, T.; Aida, T.; Someya, T. A Rubberlike Stretchable Active Matrix Using Elastic Conductors. *Science* **2008**, *321*, 1468−1472.

(5) Someya, T.; Kato, Y.; Sekitani, T.; Iba, S.; Noguchi, Y.; Murase, Y.; Kawaguchi, H.; Sakurai, T. Conformable, Flexible, Large-area Networks of Pressure and Thermal Sensors with Organic Transistor Active Matrixes. *Proc. Natl. Acad. Sci. U.S.A.* **2005**, *102*, 12321−12325.

(6) Yamada, T.; Hayamizu, Y.; Yamamoto, Y.; Yomogida, Y.; Izadi-Najafabadi, A.; Futaba, D. N.; Hata, K. A Stretchable Carbon Nanotube Strain Sensor for Human-motion Detection. *Nat. Nanotechnol.* **2011**, *6*, 296−301.

(7) Fu, Y.-F.; Li, Y.-Q.; Liu, Y.-F.; Huang, P.; Hu, N.; Fu, S.-Y. High-Performance Structural Flexible Strain Sensors Based on Graphene-Coated Glass Fabric/Silicone Composite. *ACS Appl. Mater. Interfaces* **2018**, *10*, 35503−35509.

(8) Zu, M.; Li, Q.; Wang, G.; Byun, J.-H.; Chou, T.-W. Carbon Nanotube Fiber Based Stretchable Conductor. *Adv. Funct. Mater.* **2013**, *23*, 789−793.

(9) Cheng, Y.; Wang, R.; Sun, J.; Gao, L. Highly Conductive and Ultrastretchable Electric Circuits from Covered Yarns and Silver Nanowires. *ACS Nano* **2015**, *9*, 3887−3895.

(10) Wang, Y.; Bian, K.; Hu, C.; Zhang, Z.; Chen, N.; Zhang, H.; Qu, L. Flexible and Wearable Graphene/Polypyrrole Fibers Towards Multifunctional Actuator Applications. *Electrochem. Commun.* **2013**, *35*, 49−52.

(11) Gong, J.; Lin, H.; Dunlop, J. W. C.; Yuan, J. Hierarchically Arranged Helical Fiber Actuators Derived From Commercial Cloth. *Adv. Mater.* **2017**, *29*, 1605103.

(12) Choi, D. Y.; Kim, M. H.; Oh, Y. S.; Jung, S.-H.; Jung, J. H.; Sung, H. J.; Lee, H. W.; Lee, H. M. Highly Stretchable, Hysteresis-free Ionic Liquid-based Strain Sensor for Precise Human Motion Monitoring. *ACS Appl. Mater. Interfaces* **2017**, *9*, 1770−1780.

(13) Li, Y.-Q.; Huang, P.; Zhu, W.-B.; Fu, S.-Y.; Hu, N.; Liao, K. Flexible Wire-shaped Strain Sensor from Cotton Thread for Human Health and Motion Detection. *Sci. Rep.* **2017**, *7*, 45013.

(14) Liao, X.; Liao, Q.; Zhang, Z.; Yan, X.; Liang, Q.; Wang, Q.; Li, M.; Zhang, Y. A Highly Stretchable ZnO@Fiber-Based Multifunctional Nanosensor for Strain/Temperature/UV Detection. *Adv. Funct. Mater.* **2016**, *26*, 3074−3081.

(15) Chen, S.; Wei, Y.; Wei, S.; Lin, Y.; Liu, L. Ultrasensitive Cracking-assisted Strain Sensors Based on Silver Nanowires/Graphene Hybrid Particles. *ACS Appl. Mater. Interfaces* **2016**, *8*, 25563−25570.

(16) Larson, C.; Peele, B.; Li, S.; Robinson, S.; Totaro, M.; Beccai, L.; Mazzolai, B.; Shepherd, R. Highly Stretchable Electroluminescent Skin for Optical Signaling and Tactile Sensing. *Science* **2016**, *351*, 1071−1074.

(17) Zang, Y.; Zhang, F.; Huang, D.; Gao, X.; Di, C.-a.; Zhu, D. Flexible Suspended Gate Organic Thin-film Transistors for Ultra-sensitive Pressure Detection. *Nat. Commun.* **2015**, *6*, 6269.

(18) Lee, S.; Shin, S.; Lee, S.; Seo, J.; Lee, J.; Son, S.; Cho, H. J.; Algadi, H.; Al-Sayari, S.; Kim, D. E.; Lee, T. Ag Nanowire Reinforced Highly Stretchable Conductive Fibers for Wearable Electronics. *Adv. Funct. Mater.* **2015**, *25*, 3114−3121.

(19) Lee, J.; Shin, S.; Lee, S.; Song, J.; Kang, S.; Han, H.; Kim, S.; Kim, S.; Seo, J.; Kim, D.; Lee, T. Highly Sensitive Multifilament Fiber Strain Sensors with Ultrabroad Sensing Range for Textile Electronics. *ACS Nano* **2018**, *12*, 4259−4268.

(20) Seyedin, S.; Razal, J. M.; Innis, P. C.; Jeiranikhameneh, A.; Beirne, S.; Wallace, G. G. Knitted Strain Sensor Textiles of Highly Conductive All-polymeric Fibers. *ACS Appl. Mater. Interfaces* **2015**, *7*, 21150−21158.

(21) Chen, S.; Lou, Z.; Chen, D.; Jiang, K.; Shen, G. Polymer-Enhanced Highly Stretchable Conductive Fiber Strain Sensor Used for Electronic Data Gloves. *Adv. Mater. Technol.* **2016**, *1*, 1600136.

(22) Eom, J.; Jaisutti, R.; Lee, H.; Lee, W.; Heo, J.-S.; Lee, J.-Y.; Park, S. K.; Kim, Y.-H. Highly Sensitive Textile Strain Sensors and Wireless User-interface Devices Using All-Polymeric Conducting Fibers. *ACS Appl. Mater. Interfaces* **2017**, *9*, 10190−10197.

(23) Li, X.; Hua, T.; Xu, B. Electromechanical Properties of a Yarn Strain Sensor with Graphene-sheath/Polyurethane-core. *Carbon* **2017**, *118*, 686−698.

(24) Cheng, Y.; Wang, R.; Sun, J.; Gao, L. A Stretchable and Highly Sensitive Graphene-Based Fiber for Sensing Tensile Strain, Bending, and Torsion. *Adv. Mater.* **2015**, *27*, 7365−7371.

(25) Lin, L.; Deng, H.; Gao, X.; Zhang, S.; Bilotti, E.; Peijs, T.; Fu, Q. Modified resistivity-strain behavior through the incorporation of metallic particles in conductive polymer composite fibers containing carbon nanotubes. *Polym. Int.* **2013**, *62*, 134−140.

(26) Liu, Z.; Qi, D.; Hu, G.; Wang, H.; Jiang, Y.; Chen, G.; Luo, Y.; Loh, X. J.; Liedberg, B.; Chen, X. Surface Strain Redistribution on Structured Microfibers to Enhance Sensitivity of Fiber-Shaped Stretchable Strain Sensors. *Adv. Mater.* **2018**, *30*, 1704229.

(27) Wang, H.; Liu, Z.; Ding, J.; Lepró, X.; Fang, S.; Jiang, N.; Yuan, N.; Wang, R.; Yin, Q.; Lv, W.; Liu, Z.; Zhang, M.; Ovalle-Robles, R.; Inoue, K.; Yin, S.; Baughman, R. H. Downsized Sheath-Core Conducting Fibers for Weavable Superelastic Wires, Biosensors, Supercapacitors, and Strain Sensors. *Adv. Mater.* **2016**, *28*, 4998−5007.

(28) Liu, Z. F.; Fang, S.; Moura, F. A.; Ding, J. N.; Jiang, N.; Di, J.; Zhang, M.; Lepro, X.; Galvao, D. S.; Haines, C. S.; Yuan, N. Y.; Yin, S. G.; Lee, D. W.; Wang, R.; Wang, H. Y.; Lv, W.; Dong, C.; Zhang, R. C.; Chen, M. J.; Yin, Q.; Chong, Y. T.; Zhang, R.; Wang, X.; Lima, M. D.; Ovalle-Robles, R.; Qian, D.; Lu, H.; Baughman, R. H. Hierarchically Buckled Sheath-core Fibers for Superelastic Electronics, Sensors, and Muscles. *Science* **2015**, *349*, 400−404.

(29) Iguchi, H.; Higashi, C.; Funasaki, Y.; Fujita, K.; Mori, A.; Nakasuga, A.; Maruyama, T. Rational and Practical Exfoliation of Graphite Using Well-defined Poly (3-hexylthiophene) for the Preparation of Conductive Polymer/Graphene Composite. *Sci. Rep.* **2017**, *7*, 39937.

(30) Ryu, S.; Lee, P.; Chou, J. B.; Xu, R.; Zhao, R.; Hart, A. J.; Kim, S.-G. Extremely Elastic Wearable Carbon Nanotube Fiber Strain Sensor for Monitoring of Human Motion. *ACS Nano* **2015**, *9*, 5929−5936.

(31) Hwang, J.; Jang, J.; Hong, K.; Kim, K. N.; Han, J. H.; Shin, K.; Park, C. E. Poly(3-hexylthiophene) wrapped carbon nanotube/poly(dimethylsiloxane) composites for use in finger-sensing piezoresistive pressure sensors. *Carbon* **2011**, *49*, 106−110.

(32) James, P. A.; Oparil, S.; Carter, B. L.; Cushman, W. C.; Dennison-Himmelfarb, C.; Handler, J.; Lackland, D. T.; LeFevre, M. L.;

DOI: 10.1021/acsami.9b03204
ACS Appl. Mater. Interfaces 2019, 11, 15079−15087

MacKenzie, T. D.; Ogedegbe, O.; Smith, S. C.; Svetkey, L. P.; Taler, S. J.; Townsend, R. R.; Wright, J. T.; Narva, A. S.; Ortiz, E. 2014 Evidence-Based Guideline for the Management of High Blood Pressure in Adults. *JAMA* **2014**, *311*, 507−520.

(33) Rath, N.; Balain, B. Spinal cord injury-The role of surgical treatment for neurological improvement. *J. Clin. Orthop. Trauma* **2017**, *8*, 99−102.

(34) Sanchis, M. R.; Calvo, O.; Fenollar, O.; Garcia, D.; Balart, R. Surface Modification of a Polyurethane Film by Low Pressure Glow Discharge Oxygen Plasma Treatment. *J. Appl. Polym. Sci.* **2007**, *105*, 1077−1085.

(35) Zhao, X.; Zhang, Q.; Hao, Y.; Li, Y.; Fang, Y.; Chen, D. Alternate Multilayer Films of Poly(vinyl alcohol) and Exfoliated Graphene Oxide Fabricated via a Facial Layer-by-Layer Assembly. *Macromolecules* **2010**, *43*, 9411−9416.

(36) Kim, S. J.; Mondal, S.; Min, B. K.; Choi, C.-G. Highly Sensitive and Flexible Strain-Pressure Sensors with Cracked Paddy-Shaped MoS2/Graphene Foam/Ecoflex Hybrid Nanostructures. *ACS Appl. Mater. Interfaces* **2018**, *10*, 36377−36384.

(37) Amjadi, M.; Kyung, K.-U.; Park, I.; Sitti, M. Stretchable, Skin-Mountable, and Wearable Strain Sensors and Their Potential Applications: A Review. *Adv. Funct. Mater.* **2016**, *26*, 1678−1698.

(38) Chun, S.; Kim, D. W.; Baik, S.; Lee, H. J.; Lee, J. H.; Bhang, S. H.; Pang, C. Conductive and Stretchable Adhesive Electronics with Miniaturized Octopus-Like Suckers against Dry/Wet Skin for Biosignal Monitoring. *Adv. Funct. Mater.* **2018**, *28*, 1805224.

(39) Liu, Y. F.; Li, Y. Q.; Huang, P.; Hu, N.; Fu, S. Y. On the Evaluation of the Sensitivity Coefficient of Strain Sensors. *Adv. Electron. Mater.* **2018**, *4*, 1800353.

(40) Song, H.; Zhang, J.; Chen, D.; Wang, K.; Niu, S.; Han, Z.; Ren, L. Superfast and High-sensitivity Printable Strain Sensors with Bio-inspired Micron-scale Cracks. *Nanoscale* **2017**, *9*, 1166−1173.

(41) Gong, J.; Lu, S.; Wang, R.; Cui, L. PDhms: Pulse Diagnosis via Wearable Healthcare Sensor Network. *IEEE International Conference on Communications*, 2011; pp 1−5.

DOI: 10.1021/acsami.9b03204
ACS Appl. Mater. Interfaces 2019, 11, 15079−15087